Available online at www.sciencedirect.com
SCIENCE DIRECT®
International Journal of Heat and Mass Transfer 48 (2005) 5089–5102
International Journal of HEAT and MASS TRANSFER
www.elsevier.com/locate/ijhmt

Air-side data interpretation and performance analysis for heat exchangers with simultaneous heat and mass transfer: Wet and frosted surfaces

Yanping Xia, Anthony M. Jacobi *

Department of Mechanical and Industrial Engineering, University of Illinois, 1206 West Green Street, Urbana, IL 61801, USA

Received 28 March 2005; received in revised form 5 August 2005
Available online 4 October 2005

Abstract

Data reduction methods for wet- and frosted-surface heat exchangers are reviewed, and logarithmic-mean temperature difference (LMTD) and logarithmic-mean enthalpy difference (LMED) methods for data interpretation are formulated, including fin efficiency expressions for flat-tube heat exchangers with constant-area fins. With these improved formulations for data interpretation in place, the two methods are compared using a numerical simulation of a flat-plate heat exchanger. For all conditions considered—spanning wet and frosted surfaces—the new *UA*-LMTD method provides the air-side convective heat transfer coefficient to within 3% and is more accurate than the *HA*-LMED method, which results in large errors under some conditions.

1. Introduction

When designing or predicting the performance of a heat exchanger, it is essential to relate the total heat transfer rate to the overall heat conductance and driving potential. In many air-cooling applications, condensation or frost forms on the air-side surface of a heat exchanger. For operating conditions with simultaneous sensible and latent heat transfer, two analysis methods are commonly adopted: one uses an overall heat conductance *UA* based on the logarithmic-mean temperature difference (LMTD), the other uses the so-called overall energy conductance *HA* based on the logarithmic-mean enthalpy difference (LMED). There are significant differences in these approaches and their variations reported in the literature, and these differences can lead to large differences in the heat transfer coefficient inferred from heat exchanger data, or to large departures from performance predictions. In this paper we consider data reduction and interpretation methods for heat exchangers under conditions of simultaneous heat and mass transfer. Our focus is on heat exchangers used in air-conditioning, heat pumping, and refrigeration systems.

Data reduction methods based on enthalpy potential have been widely used for condensing conditions, and several investigators have derived and used these methods for heat exchangers operating under frosting conditions. Sanders [1] presented a convincing derivation of the overall energy conductance based on an enthalpy potential. However, his expression for calculating fin efficiency unnecessarily neglects heat transfer in the frost

* Corresponding author. Tel.: +1 217 333 4108; fax: +1 217 244 6534.
E-mail addresses: xia@uiuc.edu (Y. Xia), a-jacobi@uiuc.edu (A.M. Jacobi).

0017-9310/$ - see front matter © 2005 Elsevier Ltd. All rights reserved.
doi:10.1016/j.ijheatmasstransfer.2005.08.008

Nomenclature

A	area (m^2)
c_p	specific heat ($J\ kg^{-1}\ °C^{-1}$)
g_m	mass transfer conductance ($kg\ m^{-2}\ s^{-1}$)
h	convective heat transfer coefficient ($W\ m^{-2}\ °C^{-1}$)
h_{sg}	latent heat of ablimation (for water) ($J\ kg^{-1}$)
H_f	fin height (m)
i	enthalpy ($J\ kg^{-1}$)
Δi_{lm}	logarithmic-mean enthalpy difference ($J\ kg^{-1}$)
k	thermal conductivity ($W\ m^{-1}\ °C^{-1}$)
L_f	fin width (m)
$\dot{m}$	mass flow rate ($kg\ s^{-1}$)
q	heat transfer rate (W)
R	heat transfer resistance ($°C\ W^{-1}$), or energy transfer resistance ($s\ kg^{-1}$)
t	half fin thickness, see Fig. 7 (m)
T	temperature (°C)
T_{dew}	dewpoint temperature (°C)
ΔT_{lm}	logarithmic-mean temperature difference (°C)

Greek symbols

δ	frost thickness (m)
η	fin efficiency
ω	humidity ratio

Subscripts and superscripts

1d	one-dimensional conduction effects in frost layer
a	moist air (i.e., dry air plus water vapor)
b	base
c	cold-fluid side
cond	conduction
conv	convection
f	frost
f-f	frosted-fin
fi	fin
fs	frost surface (fin surface in case of wet-surface condition)
h	hot-fluid side
i	inside/inlet
l	latent heat
o	outside/overall
r	refrigerant or coolant-side
s	sensible heat
sat	saturated
unf	unfinned
vs	accounting for variable sensible heat effects
w	tube wall

layer parallel to the length of the fin.[1] Kondepudi and O'Neal [2] derived an energy transfer coefficient in terms of the logarithmic-mean enthalpy difference, but they did not attempt to obtain the air-side convective heat transfer coefficient using the enthalpy difference. Ogawa et al. [4] used a logarithmic enthalpy difference to calculate the air-side heat transfer coefficient, but they did not separate the fin- and frost-conduction effects from the convective heat transfer coefficient. Mago and Sherif [3] calculated the overall heat transfer coefficient based on an enthalpy potential, but their method for computing the fin efficiency also neglected heat transfer in the frost layer parallel to the length of the fin.

Data interpretation using the LMED is based on several tacit assumptions, as discussed in detail later. However, the usually small error introduced by these assumptions has not been carefully quantified in earlier work. Moreover, there is a major limitation to the LMED method: it fails when the heat exchanger surface is partially wet or partially frosted. This failure occurs because mass transfer does not take place when the saturated humidity ratio corresponding to the surface temperature is higher than the humidity ratio of the moist air.

The overall energy conductance HA is commonly used to interpret heat exchanger performance for simultaneous heat and mass transfer; however, the overall heat conductance UA has been more widely adopted and often misapplied. Under frosting conditions, for example, Stoecker [5], Barrow [6], Huffman and Sepsy [7], and Niederer [8] all adopted a UA-based approach, but their use of UA follows that for dry-surface conditions (as do others). As shown later, this approach is invalid and can lead to large errors when latent heat effects are important.

In addition to difficulties in interpreting UA or HA from an LMTD or LMED analysis, respectively, the issue of wet- or frosted-fin efficiency is also not clearly resolved in the literature. Assuming a linear relation between the saturated humidity ratio and the dry-bulb temperature over the temperature range from fin tip to base, Wu and Bong [9] provided analytical solutions for fin efficiency of a straight fin operating under fully wet and partially wet conditions. For frosting conditions, some researchers, such as Stoecker [5] and Huffman and Sepsy [7], simply add another series resistance to account for the conductive resistance of the

[1] As shown later, the fin efficiency expression developed by Sanders [1] (as described in [13]) has an error.

frost. However, such a model neglects temperature variations along the frost surface, and the effects of such a simplification can be profound (see Xia and Jacobi [10]). Similar to the work of Sanders [1], Kondepudi and O'Neal [11] assumed no heat transfer in the frost layer along the fin length, and they developed an expression for fin efficiency for pin-fin heat exchangers under frosting conditions. They used an effective heat transfer coefficient, including latent and sensible heat transfer in the air-side convection coefficient.

In order to avoid the error associated with neglecting conduction heat transfer in the frost layer along the direction of the fin length, Xia and Jacobi [10] solved the heat conduction equation for a composite medium consisting of a two-dimensional frost layer on a one-dimensional fin. They provided a simplified, one-term analytical solution for the fin efficiency, valid over a wide range of conditions, including most frost-coated metallic fins. An effective heat transfer coefficient is also needed in their model, and such an approach is justified if the sensible heat ratio is constant over the surface (this restriction is discussed later in detail).

The technical literature is replete with methods for reducing heat exchanger data under conditions of simultaneous heat and mass transfer. While the conventional approaches of *UA*-LMTD and *HA*-LMED and simple adaptations to dry-fin efficiency calculations are appropriate under some conditions, they can introduce large errors under other conditions. In this paper, valid LMTD and LMED approaches for wet- and frosted-surface heat transfer will be clearly formulated—with attention to errors in conventional application of the methods—and expressions for fin efficiency will be provided for both methods. With improved formulations for data interpretation in place, the two methods will be compared and evaluated using a numerical simulation of a heat exchanger. A rational and consistent approach to reducing heat exchanger data might resolve (and avoid) disagreement over the behavior of the heat transfer coefficient under wet- and frosted-surface conditions.

2. Problem description

The purpose is to formulate rational, general, and convincing methods for data reduction and interpretation applicable for wet- or frosted-surface heat exchangers. The development will focus on constant-area (straight) fins; however, an extension to other fins is obvious. The purpose of the data reduction is to obtain the air-side convective heat transfer coefficient from measurements of air inlet and outlet dry- and wet-bulb temperatures, coolant inlet and outlet temperatures, and air and coolant mass flow rates. The tube-wall conduction resistance is neglected, because it is almost always negligible, and the focus is now on the air-side resistance. The formulation of both the *UA*-LMTD and *HA*-LMED methods is presented in the sections that follow.

3. Logarithmic-mean enthalpy difference method

The energy transfer network for a heat exchanger working under wet or frosting conditions is shown in Fig. 1(a). The form of this network, and part of the appeal of this formulation, is that it is directly analogous to the dry-surface network, with a series of resistors between two enthalpies, analogous to a series of resistors between two temperatures.

In this network, the widely accepted concept of enthalpy potential is used, as described in Stoecker and Jones [12]. The heat transfer from the free-stream air to the wet surface is expressed in the form of enthalpy potential, i.e.,

$$\mathrm{d}q_\mathrm{a} = \mathrm{d}A\,\frac{h}{c_{p_\mathrm{a}}}(i_\mathrm{a} - i_\mathrm{fs}). \tag{1}$$

In developing Eq. (1), the analogy between heat and mass transfer is used with $Le^n \approx 1$, and with $i_\mathrm{f}(\omega_\mathrm{fs} - \omega_\mathrm{a})$ neglected, where Le is Lewis number (Pr/Sc) and i_f is the enthalpy of saturated liquid water (see Stoecker and Jones [12]). By assuming $Le^n \approx 1$, an error in $\mathrm{d}q_\mathrm{a}$ of about 8% can be introduced at a latent heat ratio of 50% (with $Le \approx 1.25$); this approximation is the major source of error in the LMED method.

In Eq. (1), the enthalpy at the wet surface, i_fs, is taken as that of saturated moist air at the surface temperature. Also, in Fig. 1(a), all the enthalpies except the enthalpy of the free-stream air, i_a, are evaluated as the enthalpy of saturated air at each corresponding temperature. In order to derive an expression for fin efficiency and the convective resistance of the coolant flow, $R_\mathrm{r,conv}$, a linearization between the saturation enthalpy and the temperature of moist air is utilized, following Sanders [1]:

$$i = a + bT, \tag{2}$$

where a and b are the coefficients for the linearization. This linearization, within the range of the operating temperatures, approximates the value of saturation enthalpy, and introduces another source of error. Based on the above assumptions, an overall energy conductance HA can be derived, as shown by Kondepudi and O'Neal [2]:

$$HA = \frac{q_\mathrm{a}}{\Delta i_\mathrm{lm}}, \tag{3}$$

where Δi_lm is the logarithmic-mean enthalpy difference. Δi_lm takes different forms for different heat exchanger flow arrangements (e.g., parallel flow and counter flow). Neglecting the conduction resistance of the tube wall, we have

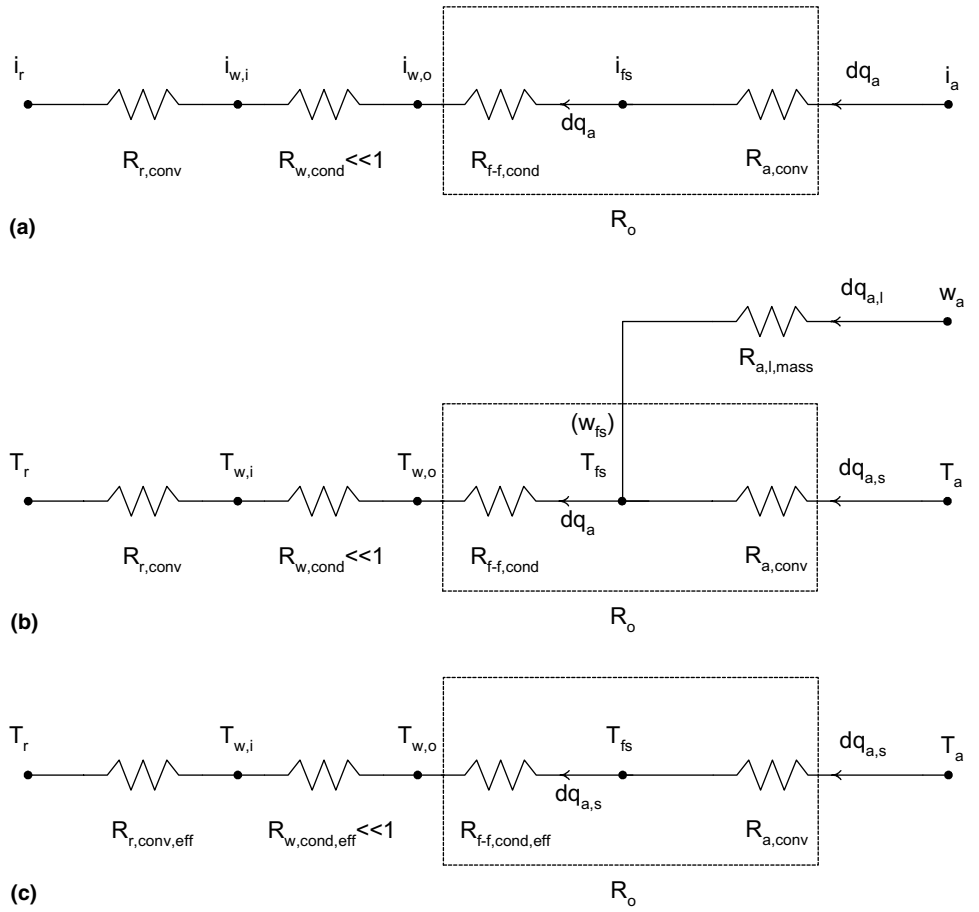

Fig. 1. The energy transfer network (a), heat and mass transfer network (b), and analogous heat transfer network (c) with respect to an infinitesimal heat transfer area dA_h (or corresponding dA_c) for a heat exchanger operating under wet or frosting conditions.

$$\frac{1}{HA} = R_{r,conv} + R_o = \frac{1}{A_c h_c / b} + \frac{1}{\eta_h A_h h_h / c_{p_a}}. \quad (4)$$

Eqs. (3) and (4) constitute *HA*-LMED method. It should be noted that if the humidity ratio corresponding to the surface temperature is higher than that of the air, no mass transfer occurs, because there is no condensate or frost on the surface. Thus, Eq. (1) is restricted to having mass transfer to occur only from the moist air stream *to* the surface. Neglecting this restriction causes the heat transfer calculated from Eq. (1) to erroneously include latent heat associated with impossible mass transfer from the (dry) surface to the air; as shown later, this error results in unrealistically high values of the heat transfer coefficient to be inferred from heat exchanger performance data. The *HA*-LMED method is applicable only when the surface is fully wet or frosted, and application to a partially wet or frosted surface requires area partitioning and a *UA*-LMTD analysis of the dry portion of the heat exchanger.

Next, expressions for fin efficiency and overall surface efficiency will be developed. The overall surface efficiency and fin efficiency, respectively, are

$$\eta_h = \frac{q_a}{A_h (h_h / c_{p_a})(i_a - i_{w,o})} \quad (5)$$

and

$$\eta = \frac{q_{fi,b}}{A_{fi} (h_h / c_{p_a})(i_a - i_{w,o})}, \quad (6)$$

where $q_{fi,b}$ is the total heat (sensible and latent heat) flowing through the base of the fin, or the composite fin (fin plus frost) for the cases of frosting conditions. The derivations of η and η_h for frosting conditions are provided in Appendix A. The final expression for fin efficiency under frosting conditions is

$$\eta = \frac{2}{h_h (b/c_{p_a}) H_f \delta_f} \sum_{n=1}^{\infty} C_n \lambda_n \sin h\left(\frac{\lambda_n H_f}{2\delta_f}\right) \times \left\{ k_{fi} t + k_f \delta_f \left[\frac{\sin(\lambda_n)}{\lambda_n} + \frac{k_{fi} t}{k_f \delta_f} (\cos(\lambda_n) - 1) \right] \right\} \quad (7a)$$

with

$$C_n = \frac{2\left(\frac{\sin(\lambda_n)/\lambda_n}{\cosh(\lambda_n H_f/2\delta_f)} + \frac{k_{fi}t}{k_f\delta_f}\frac{\cos(\lambda_n)}{\cosh(\lambda_n H_f/2\delta_f)}\right)}{1+\frac{\sin(2\lambda_n)}{2\lambda_n}+\left(\frac{k_{fi}t}{k_f\delta_f}\right)^2\lambda_n^2\left[1-\frac{\sin(2\lambda_n)}{2\lambda_n}\right]+\frac{k_{fi}t}{k_f\delta_f}[1+\cos(2\lambda_n)]} \tag{7b}$$

and λ_n is the root of

$$\tan(\lambda_n) = \frac{k_{fi}k_f t}{\delta_f\left(k_f^2 + (h_h b/c_{p_a})k_{fi}t\right)}\left[\left(\frac{(h_h b/c_{p_a})\delta_f^2}{k_{fi}t}\right)\frac{1}{\lambda_n} - \lambda_n\right]. \tag{7c}$$

A one-term approximation to the fin efficiency is (see [10])

$$\eta = \frac{2\lambda}{h_h(b/c_{p_a})H_f\delta_f}\tanh\left(\frac{\lambda H_f}{2\delta_f}\right)(k_{fi}t + k_f\delta_f), \tag{8a}$$

with

$$\lambda = \delta_f\sqrt{\frac{h_h(b/c_{p_a})}{k_{fi}t + \delta_f\left[k_{fi}h_h(b/c_{p_a})t/k_f + k_f\right]}}. \tag{8b}$$

Alternately, if conduction heat transfer in the frost layer parallel to the length of the fin is neglected, the expressions of η and λ can be shown to reduce to

$$\eta_{1d} = \frac{2\lambda_{1d}}{h_h(b/c_{p_a})H_f\delta_f}\tanh\left(\frac{\lambda_{1d}H_f}{2\delta_f}\right)(k_{fi}t), \tag{9a}$$

with

$$\lambda_{1d} = \delta_f\sqrt{\frac{h_h(b/c_{p_a})}{k_{fi}t + \delta_f\left[k_{fi}h_h(b/c_{p_a})t/k_f\right]}}. \tag{9b}$$

Finally, the surface efficiency is

$$\eta_h = \eta\frac{A_{fi}}{A_h} + \left(\frac{k_f/\delta_f}{h_h(b/c_{p_a}) + k_f/\delta_f}\right)\frac{A_h - A_{fi}}{A_h}. \tag{10}$$

Comparing Eq. (9) to the expression of Sanders [1] as presented by Kondepudi and O'Neal [13], it can be seen that the fin efficiency as developed by Sander is incorrect; the error leads to the misleading conclusion that fin efficiency increases with increasing frost thickness. In Fig. 2, η and η_{1d} are compared using the parametric values of Table 1 and $(b/c_{p_a}) = 1.3$, representing moist air at $-20 < T < 0$ °C and $0 < \mathrm{RH} < 80\%$. The values obtained by numerically solving the governing equations given in Appendix A (Eqs. (A.5) and (A.6)), are also shown in Fig. 2, providing the 'true' fin efficiency. As frost grows, the frosted-fin efficiency decreases, and the error in η_{1d} Eq. (9) becomes larger, because of neglected heat conduction in the frost layer parallel to the fin length. The error exceeds 2% for frost thicker than $\delta = 1$ mm. For frost layers with $\delta < 1$ mm, the one-term approximation (Eq. (8)) may be used, but for $\delta > 1$ mm at least two terms in Eq. (7) are required to keep errors in η below 2%.

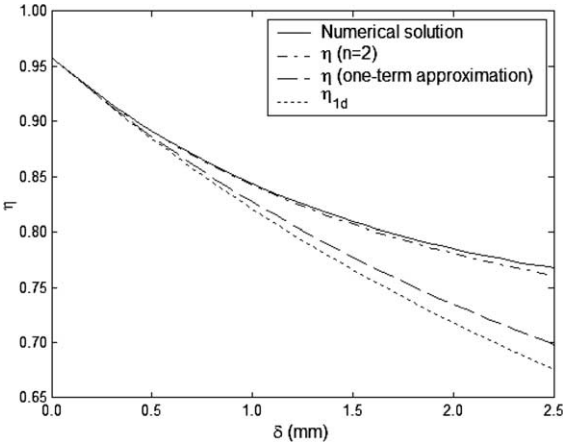

Fig. 2. A comparison of frosted fin efficiency, η, as calculated by a finite-difference numerical solution (see [10]), the analytical solution given by Eq. (7) with $n = 2$, the one-term approximation to the analytical solution given by Eq. (8), and the one-dimensional approximation given by Eq. (9) for η_{1d}.

Table 1
Parameters used in Figs. 2 and 3

H_f mm	8.28
h_h W m^{-2} K^{-1}	70.4
k_{fi} W m^{-1} K^{-1}	237
k_f W m^{-1} K^{-1}	0.525
t mm	0.05

A derivation similar to that outlined in Appendix A results in expressions for condensing conditions that can be obtained by replacing h with hb/c_{p_a} in the expressions for dry-fin efficiency; thus for condensing conditions

$$\eta = \frac{\tanh(\lambda H_f/2)}{\lambda H_f/2}, \tag{11}$$

with [1]

$$\lambda = \sqrt{\frac{h_h(b/c_{p_a})}{k_{fi}t}} \tag{12}$$

and

$$\eta_h = 1 - \frac{A_{fi}}{A_h}(1-\eta). \tag{13}$$

4. Logarithmic-mean temperature difference method

A valid heat and mass transfer network for a heat exchanger operating under wet- or frosted-surface conditions is shown in Fig. 1(b). We can cast the network of Fig. 1(b) into a form analogous to that of Fig. 1(a)

if we define an *effective* heat transfer resistance to be the temperature difference over sensible heat transfer. The resulting network is then reduced to the one shown in Fig. 1(c); this form of resistor network is convenient and appealing because of its similarity to the dry-surface and LMED networks. As an example of an effective resistance, consider the effective convective heat transfer resistance on the coolant side, $R_{r,conv,eff}$:

$$R_{r,conv,eff} = \frac{T_{w,i} - T_r}{q_{a,s}}. \tag{14}$$

Then, following the approach used in dry-surface heat exchanger analysis, an overall heat transfer coefficient is defined as

$$U = \frac{dq_{a,s}}{dA_h \Delta T} = \frac{dq_{a,s}}{dA_h (T_a - T_r)}. \tag{15}$$

Based on Fig. 1(c), the resistance components in the network are

$$\frac{1}{U dA_h} = R_{r,conv,eff} + R_o = \frac{1}{dA_c h_c (dq_{a,s}/dq_a)} + \frac{1}{\eta_h dA_h h_h}. \tag{16}$$

The appropriate UA-LMTD method is derived by relating the heat transfer rates to the temperature changes on the air and the refrigerant side,

$$dq_a = \dot{m}_r c_{p_r} dT_r, \tag{17}$$

and

$$dq_{a,s} = -\dot{m}_a c_{p_a} dT_a. \tag{18}$$

Noting $\Delta T = T_a - T_r$, we have

$$d(\Delta T) = dT_a - dT_r. \tag{19}$$

Substituting from Eqs. (17) and (18) into Eq. (19):

$$d(\Delta T) = -dq_{a,s}\left[\frac{1}{\dot{m}_a c_{p_a}} + \frac{1}{\dot{m}_r c_{p_r} (dq_{a,s}/dq_a)}\right]. \tag{20}$$

From the definition of U, recognizing we will base the overall conductance on the air-side area (i.e., UA_h), we have

$$dq_{a,s} = U dA_h \Delta T. \tag{21}$$

Substituting into Eq. (20), rearranging, and noting that $d(\Delta T)/\Delta T = d(\ln \Delta T)$,

$$d(\ln \Delta T) = -U dA_h\left[\frac{1}{\dot{m}_a c_{p_a}} + \frac{1}{\dot{m}_r c_{p_r} (dq_{a,s}/dq_a)}\right]. \tag{22}$$

In general, the local sensible heat ratio $dq_{a,s}/dq_a$ can be expected to vary over the surface area, and expressing it analytically to pursue a closed-form integration of Eq. (22) requires assumptions that vitiate the generality of the resulting solution. However, when the variation in $dq_{a,s}/dq_a$ is negligible the local sensible heat ratio is equal to $q_{a,s}/q_a$, and Eqs. (20) and (22) can be easily integrated, and combining by eliminating the term in the square bracket gives

$$UA = \int U\, dA_h = \frac{q_{a,s}}{\Delta T_{lm}}, \tag{23}$$

where ΔT_{lm} is the logarithmic-mean temperature difference. ΔT_{lm} takes a form dependent on flow arrangement of the heat exchanger. Because this convenient form results, we will adopt the assumption that $dq_{a,s}/dq_a = q_{a,s}/q_a$ (equivalent to assuming variations in $dq_{a,s}/dq_a$ negligible); in evaluating the method later in the paper, we will explore the impact of deviations from that assumption on the inferred heat transfer coefficient. Under this assumption, Eq. (16) yields

$$\frac{1}{UA} = \frac{1}{A_c h_c (q_{a,s}/q_a)} + \frac{1}{\eta_h A_h h_h}. \tag{24}$$

Eqs. (23) and (24) constitute the method of UA-LMTD. The method also applies to dry-surface conditions, where $dq_{a,s}/dq_a = q_{a,s}/q_a = 1$ and Eqs. (23) and (24) reduce to those of dry test conditions. The particularly interesting cases of partially wet- or frosted-surface conditions will also be assessed in the next section—those cases represent extreme departures from the $dq_{a,s}/dq_a = q_{a,s}/q_a$.

The remaining task is to develop expressions for fin efficiency and overall surface efficiency. The overall surface efficiency is defined as

$$\eta_h = \frac{q_a}{A_h h_h (q_a/q_{a,s})(T_a - T_{w,o})}. \tag{25}$$

For frosting conditions, the fin efficiency is defined as the ratio of the total heat flowing through the base of the composite fin (fin plus frost), to the maximum possible total heat that can be exchanged were the surface temperature of the composite fin at the fin base temperature. Invoking the assumption of constant sensible heat ratio again, the definition of this frosted-fin efficiency can be reduced to

$$\eta = \frac{q_{fi,b}}{A_{fi} h_h (q_a/q_{a,s})(T_a - T_{w,o})}. \tag{26}$$

The derivation of η and η_h are provided in Appendix A. The final expressions for frosting conditions are

$$\eta = \frac{2}{h_h (q_a/q_{a,s}) H_f \delta_f} \sum_{n=1}^{\infty} C_n \lambda_n \sinh\left(\frac{\lambda_n H_f}{2\delta_f}\right) \times \left\{k_{fi} t + k_f \delta_f \left[\frac{\sin(\lambda_n)}{\lambda_n} + \frac{k_{fi} t}{k_f \delta_f}(\cos(\lambda_n) - 1)\right]\right\} \tag{27a}$$

with C_n calculated using Eq. (7b), and λ_n being the root of

$$\tan(\lambda_n) = \frac{k_{fi} k_f t}{\delta_f (k_f^2 + (h_h q_a/q_{a,s}) k_{fi} t)} \times \left[\left(\frac{(h_h q_a/q_{a,s})\delta_f^2}{k_{fi} t}\right)\frac{1}{\lambda_n} - \lambda_n\right]. \tag{27b}$$

A one-term approximation to the fin efficiency is (see [10])

$$\eta = \frac{2\lambda}{h_h(q_a/q_{a,s})H_f\delta_f}\tanh\left(\frac{\lambda H_f}{2\delta_f}\right)(k_{fi}t + k_f\delta_f), \tag{28a}$$

where

$$\lambda = \delta_f\sqrt{\frac{h_h(q_a/q_{a,s})}{k_{fi}t + \delta_f\left[k_{fi}h_h(q_a/q_{a,s})t/k_f + k_f\right]}}. \tag{28b}$$

Finally, the surface efficiency is

$$\eta_h = \eta\frac{A_{fi}}{A_h} + \left(\frac{k_f/\delta_f}{h_h(q_a/q_{a,s}) + k_f/\delta_f}\right)\frac{A_h - A_{fi}}{A_h}. \tag{29}$$

Similarly, the expressions of η and η_h for condensing conditions are

$$\eta = \frac{\tanh(\lambda H_f/2)}{\lambda H_f/2}, \tag{30}$$

where

$$\lambda = \sqrt{\frac{h_h(q_a/q_{a,s})}{k_{fi}t}} \tag{31}$$

and

$$\eta_h = 1 - \frac{A_{fi}}{A_h}(1-\eta). \tag{32}$$

In the above expressions for fin efficiency, the mass transfer effects are absorbed into the air-side heat transfer coefficient by assuming a constant sensible heat ratio. More accurate expressions can be developed if the mass transfer effects are isolated by assuming a linear relation between the saturated humidity ratio ω_{sat} and moist-air temperature T over the temperature range from fin tip to fin base, i.e.,

$$\varpi_{sat} = c + eT. \tag{33}$$

where c and e are constants for the linearization. Invoking this assumption is equivalent to assuming a linear relationship between the sensible heat and the total heat over the fin surface. Wu and Bong [9] used this assumption to develop fin efficiency expressions for condensing conditions. Our new derivation for frosting conditions is given in Appendix A; the resulting expressions for fin efficiency are

$$\eta_{vs} = \frac{2}{h'_hH_f\delta_f}\sum_{n=1}^{\infty}C_{n,vs}\lambda_{n,vs}\sinh\left(\frac{\lambda_{n,vs}H_f}{2\delta_f}\right) \times\left\{k_{fi}t + k_f\delta_f\left[\frac{\sin(\lambda_{n,vs})}{\lambda_{n,vs}} + \frac{k_{fi}t}{k_f\delta_f}(\cos(\lambda_{n,vs}) - 1)\right]\right\} \tag{34a}$$

with $C_{n,vs}$ calculated using Eq. (7b) and $\lambda_{n,vs}$, and $\lambda_{n,vs}$ is the root of

$$\tan(\lambda_{n,vs}) = \frac{k_{fi}k_ft}{\delta_f(k_f^2 + h'_hk_{fi}t)}\left[\left(\frac{h'_h\delta_f^2}{k_{fi}t}\right)\frac{1}{\lambda_{n,vs}} - \lambda_{n,vs}\right] \tag{34b}$$

and

$$h'_h = h_h\left(1 + \frac{h_{sg}g_me}{h_h}\right). \tag{35}$$

A one-term approximation is (see [10])

$$\eta_{vs} = \frac{2\lambda_{vs}}{h'_hH_f\delta_f}\tanh\left(\frac{\lambda_{vs}H_f}{2\delta_f}\right)(k_{fi}t + k_f\delta_f), \tag{36a}$$

with

$$\lambda_{vs} = \delta_f\sqrt{\frac{h'_h}{k_{fi}t + \delta_f[k_{fi}h'_ht/k_f + k_f]}}. \tag{36b}$$

In Fig. 3, the values of η and η_{vs} are compared for the parametric values given in Table 1, with a frost thickness of 1 mm for various values of relative humidity. The values of mass transfer conductance, g_m, are related to the convective heat transfer coefficients, h_h, through the Lewis analogy. The values obtained by numerically solving the governing equations for the temperature distribution in the frosted fin, as given in Appendix A (Eqs. (A.1)–(A.3) as appropriate), which closely represents the true fin efficiency, are also shown in Fig. 3. In Fig. 3a, results from using Eqs. (27) and (34) with $n = 2$ are shown, and the one-term approximations given by Eqs. (28) and (36) are shown in Fig. 3b. Clearly, the use of η_{vs} is superior to that of η: it predicts fin-efficiency and trends better, because it accounts for the variation of saturation state on the fin. The relative-humidity conditions for which no mass transfer occurs, and for which the fin is partially frosted are also shown. In application, if a fin is partially frosted, a portion of the fin area is frost-coated, and the coverage would change in time. If it is desired to reduce heat exchanger data with insensitivity to partially frosted or partially wet conditions, and with fin efficiency errors of less than 1%, then Eq. (34) should be adopted. It should be noted, however, that the errors associated with the much simpler Eq. (28) or (36) are less than about 2%, and not much accuracy is sacrificed by their use.

5. An evaluation of the two methods

An evaluation of the two methods, *HA*-LMED and *UA*-LMTD, will be conducted using a numerical model of a parallel-plate heat exchanger operating in a parallel-flow configuration. We adopt this approach because the fin-efficiency models have been validated, and the focus is now on assessing the impact of the fundamental assumptions of the two methods. For simplicity, the simulation of frosting conditions is conducted at the quasi-steady-state condition corresponding to the start of frosting; i.e., there is not a resistance due to frost in the numerical model. In addition to the conservation

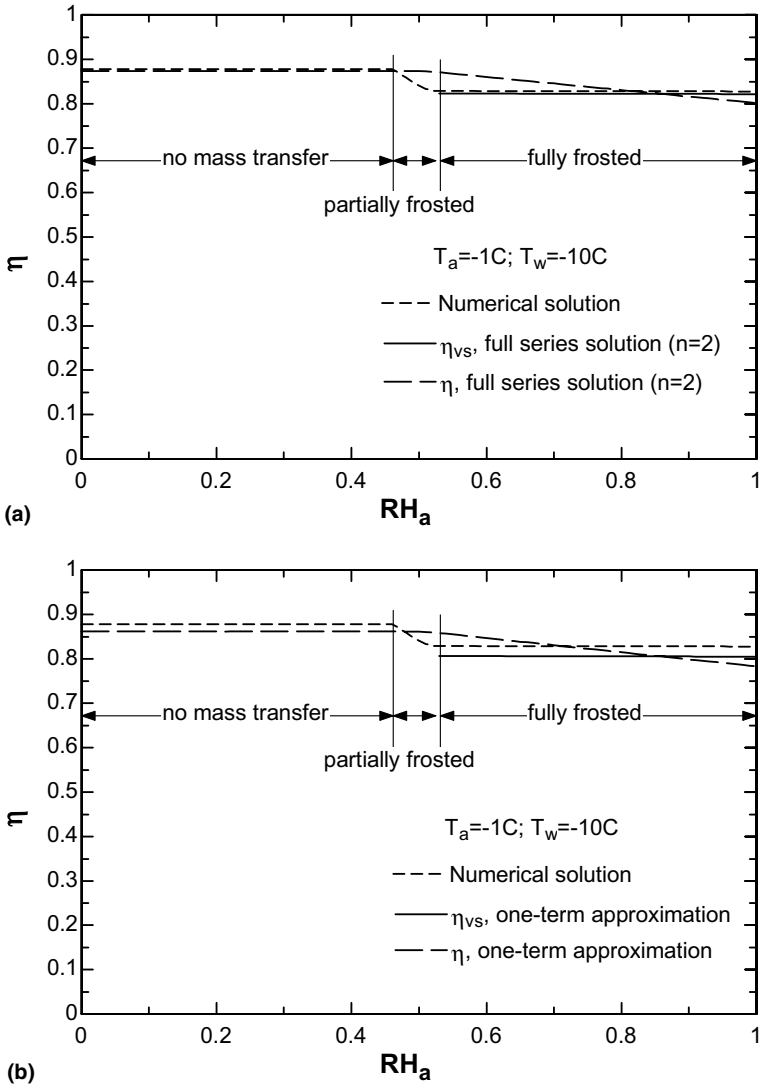

Fig. 3. A comparison between η, η_{vs} and the numerical solution of fin efficiency: (a) using the series solutions with $n = 2$, and (b) using a one-term approximation.

of energy, as expressed by Eqs. (17) and (18), the rate equations for simultaneous heat and mass transfer are needed. They are

$$dq_{a,s} = dA_h h_h (T_a - T_w), \tag{37}$$

$$dq_{a,l} = \begin{cases} dA_h h_{sg} g_m (\varpi_a - \varpi_w), & \varpi_a > \varpi_w, \\ 0, & \varpi_a \leqslant \varpi_w, \end{cases} \tag{38}$$

$$dq_a = dA_c h_c (T_w - T_r), \tag{39}$$

$$dq_a = dq_{a,s} + dq_{a,l}, \quad \text{and} \tag{40}$$

$$dq_{a,l} = -\dot{m}_a h_{sg} d\varpi_a. \tag{41}$$

Eqs. (17), (18), and (37)–(41) are the governing equations, and a real-mixture psychrometric relationship gives the saturated humidity ratio as a function of the local plate temperature, $\omega_w(T_w)$, at one atmosphere. Noting $dA_c = dA_h$, the inlet air and coolant temperatures and the inlet humidity, along with air- and coolant-side convection coefficients and flow rates are prescribed. The governing equations are solved numerically to find the outlet temperatures, humidity, sensible, latent, and total heat transfer. The numerical solution was based on a central-difference approximation to the derivatives, with a varying discretization of the heat transfer area.[2]

[2] In Figs. 4–6, six area elements were used (to allow easy interpretation of the local sensible heat ratio). In Table 3, 50 area elements were used. The numerical uncertainty is less than $\pm 0.3\ W\ m^{-2}\ K^{-1}$ for the six-element case and less than $\pm 10^{-5}\ W\ m^{-2}\ K^{-1}$ for the results in Table 3.

Table 2
Parameters used in the numerical simulation

h_h W m^{-2} K^{-1}	50
$\dot{m}_a$ kg/s	0.15
$\dot{m}_r$ kg/s	0.105
A_h m^2	3
A_c m^2	3

With the inlet and outlet temperatures and humidity taken as known, along with the flow rates and the coolant-side convection coefficient, the air-side heat transfer coefficient is calculated using the *HA*-LMED and *UA*-LMTD methods developed in the prior sections. The results are in turn compared to the value prescribed in the numerical model (taken as the 'true' value). These tests were conducted over a range of temperatures, relative humidities, and coolant-side convection coefficients. The parameters taken as fixed in all the simulations are provided in Table 2. The coolant properties were taken as those of ethyl alcohol. The conditions for these numerical tests were adopted to mimic application;

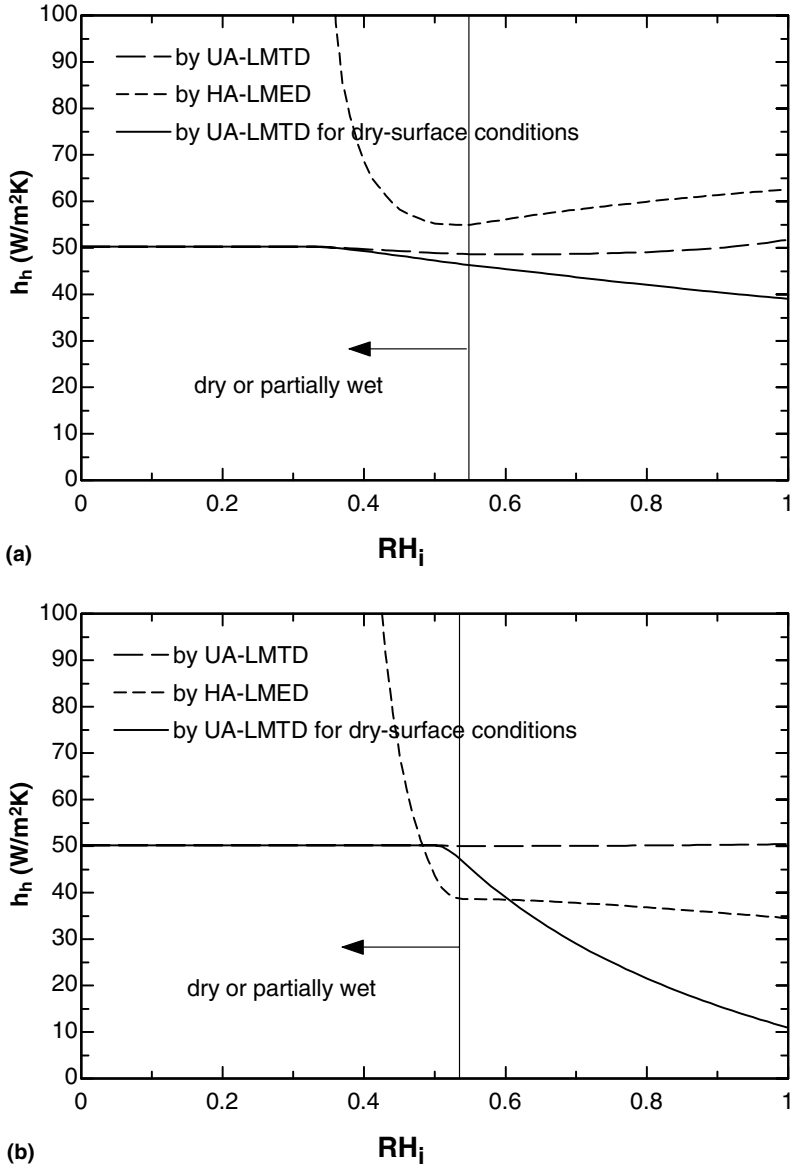

Fig. 4. A comparison between the inferred air-side convective heat transfer coefficients from the methods of *HA*-LMED and *UA*-LMTD for air-conditioning conditions, when the true value is $h_h = 50$ W m^{-2} K^{-1} (with $T_{a,i} = 27$ °C and $T_{r,i} = 7$ °C): (a) $h_c/h_h = 10$; (b) $h_c/h_h = 1$.

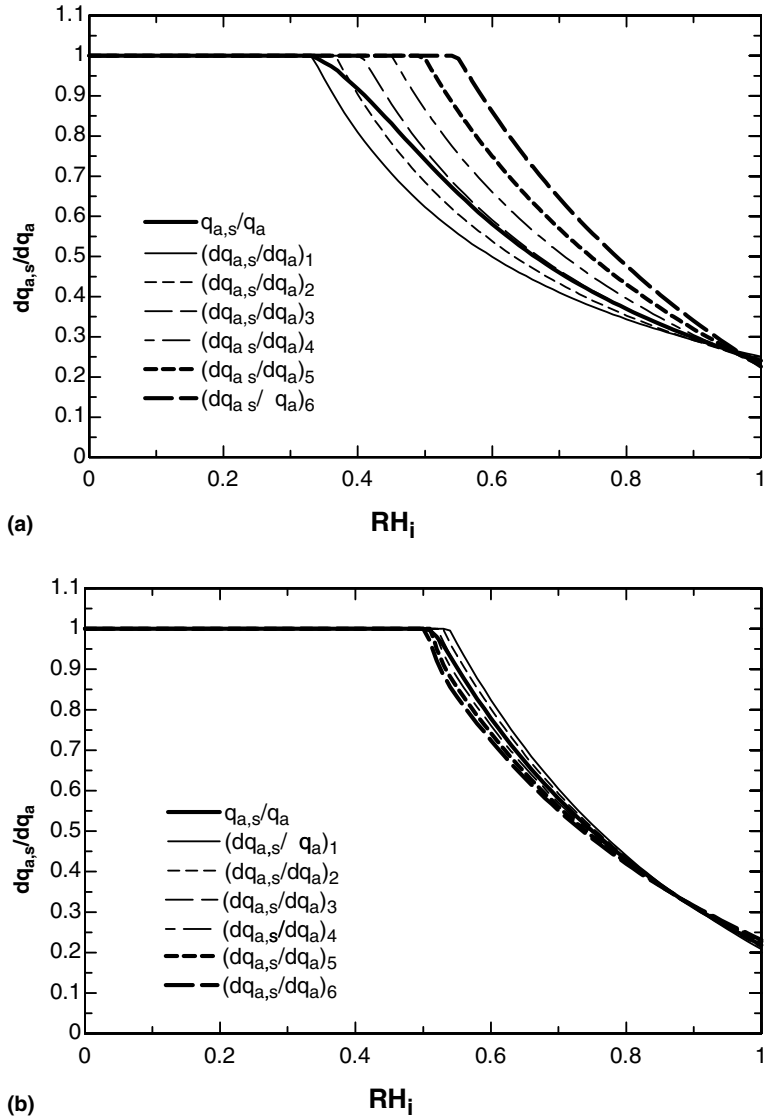

Fig. 5. The variation in local sensible heat ratios corresponding to Fig. 4.

restrictions notwithstanding, the results are general as a basis for understanding and evaluating the *HA*-LMED and *UA*-LMTD methods.

The calculated air-side heat transfer coefficient for varying inlet humidity is shown in Fig. 4 for two different h_c/h_h ratios under air-conditioning conditions; the corresponding variations in local sensible heat ratio are shown in Fig. 5. The air-side convective heat transfer coefficient calculated using the method of *UA*-LMTD for dry-surface conditions, i.e., with Eq. (24) replaced by

$$\frac{1}{UA}=\frac{1}{A_c h_c}+\frac{1}{\eta_h A_h h_h}, \tag{42}$$

is also shown in Fig. 4. As described earlier, it is not uncommon for this approach to be adopted in interpreting wet- and frosted-surface heat exchanger data. However, it is clear from the results that misapplication of Eq. (42) can result in very large errors, especially at high relative humidity. It is also evident that if the *HA*-LMED method is used for dry or partially wet conditions, unrealistic predictions result. Under dry-surface conditions, the heat transfer coefficient calculated using the *UA*-LMTD method developed in this paper approaches the true value ($50\ \mathrm{W\,m^{-2}\,K^{-1}}$). For partially or fully wet conditions, although the variation in the local sensible heat ratio can be significant—as shown in Fig. 5(a)—the error in the calculated heat transfer

coefficient is small (less than 3%). The tolerance of the *UA*-LMTD method to variation in $dq_{a,s}/dq_a$ is probably because $q_{a,s}/q_a$ is weighted by the local heat transfer rates integrated over area. This weighting is apparent in Fig. 5(a), where $q_{a,s}/q_a$ is closer to the local values near the heat exchanger inlet, where heat transfer rates are higher. This natural weighting by heat transfer rate, when extracting a rate coefficient, mitigates the impact of local variations, because the local values of $dq_{a,s}/dq_a$ departing the most from $q_{a,s}/q_a$ are weighted the least. Nevertheless, by comparing Figs. 4(a) and 5(a) to 4(b) and 5(b), it is evident that the smaller the variation in $dq_{a,s}/dq_a$, the smaller the error in the calculated heat transfer coefficient by *UA*-LMTD.

Example results for frosting conditions are provided in Fig. 6, where the calculated air-side heat transfer coefficients and variation in local sensible heat ratio are given for $h_c/h_h = 10$. For all the conditions shown, the *UA*-LMTD method provides much more accurate results than the *HA*-LMED method.

The maximum relative deviation in local sensible heat ratio with respect to the total sensible heat ratio, and the relative errors in the air-side heat transfer coefficient calculated using *HA*-LMED and *UA*-LMTD for conditions typical to air conditioning, heat pumping, medium-temperature refrigeration (M-R), and low-temperature refrigeration (L-R) are given in Table 3. Results are provided for three different h_c/h_h and two different total

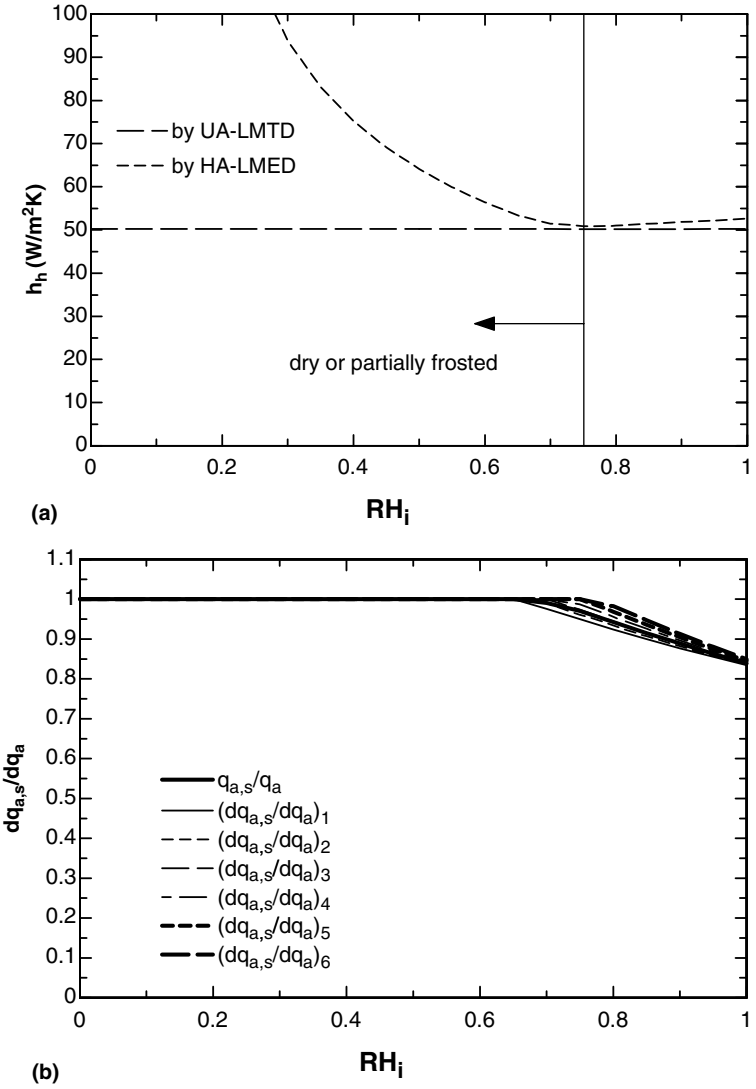

Fig. 6. The calculated air-side convective heat transfer coefficients, when the true value is $h_h = 50\ W\ m^{-2}\ K^{-1}$ (a), and the variation in local sensible heat ratio (b) for low-refrigeration conditions ($T_{a,i} = -18\ °C$ and $T_{r,i} = -23\ °C$) with $h_c/h_h = 10$.

Table 3
The relative errors in the air-side heat transfer coefficient calculated using *HA*-LMED and *UA*-LMTD for typical evaporator operating conditions (NA denotes partially wet/frosted or dry conditions; parameters provided in Table 2 were used unless otherwise specified)

Test conditions ($T_{r,i}$, $T_{a,i}$, $T_{dew,i}$) [°C]		$\frac{h_c}{h_h}$	A_h [m^2]	$\max\left\lvert\frac{dq_{a,s}/dq_a - q_{a,s}/q_a}{q_{a,s}/q_a}\right\rvert \times 100[\%]$	$\left\lvert\frac{h_{h,LMED} - h_h}{h_h}\right\rvert \times 100[\%]$	$\left\lvert\frac{h_{h,LMTD} - h_h}{h_h}\right\rvert \times 100[\%]$
Condensing	A-C (7, 27, 15)	10	0.6	5.5	7.0	0.11
			3	28	NA	2.5
		1	0.6	0	NA	0.0043
			3	0	NA	0.0013
	H-P (0, 8, 4)	10	0.6	3.0	7.2	0.055
			3	28	NA	1.8
		1	0.6	1.1	8.2	0.016
			3	5.9	5.7	0.17
		0.1	0.6	0	NA	0.032
			3	0	NA	0.032
Frosting	M-R (−7, 2, 0)	10	0.6	1.0	9.9	0.013
			3	13	9.5	0.95
		1	0.6	0.089	2.9	0.011
			3	0.36	0.67	0.023
		0.1	0.6	0	NA	0.032
			3	0	NA	0.032
	L-R (−23, −18, −20)	10	0.6	0.50	2.4	0.00021
			3	4.4	1.8	0.30
		1	0.6	0.15	0.37	0.011
			3	0.75	0.074	0.029
		0.1	0.6	0	NA	0.032
			3	0	NA	0.032
	H-P (−17, −8, −9)	10	0.6	0.25	6.8	0.0057
			3	3.5	6.8	0.25
		1	0.6	0.30	1.6	0.0084
			3	1.6	2.5	0.035
		0.1	0.6	0	NA	0.032
			3	9.5	NA	1.3

heat transfer areas. In general, the error in the method of *UA*-LMTD is within 3%, and is smaller than *HA*-LMED for all conditions.

6. Summary and conclusions

Valid *HA*-LMED and *UA*-LMTD methods for wet- and frosted-surface heat transfer were formulated. Fin-efficiency expressions for flat-tube heat exchangers with constant-area fins are provided for both methods, with improved expressions for frosted-surface conditions that consider two-dimensional conduction of heat in the frost layer. The *UA*-LMTD method is shown to provide the best results for dry, partially wet/frosted, and fully wet/frosted conditions. The *HA*-LMED method is only applicable to fully wet/frosting conditions. For all the conditions considered, the *UA*-LMTD method provided the value of the air-side convective heat transfer coefficient within 3% and is more accurate than the method of *HA*-LMED.

Acknowledgements

This work received financial support from the Air-Conditioning and Refrigeration Technology Institute (ARTI) under 21-CR, Elizabeth Jones program director, and from the Air Conditioning and Refrigeration Center, an NSF-founded Industry-University Cooperative Research Center. Their support is gratefully acknowledged.

Appendix A

The physical situation of interest, frost on a metallic fin, is shown in Fig. 7(a). The dashed box, enlarged in Fig. 7(b), shows in detail the physical system. The metallic fin and the frost slab form a composite medium. The convection coefficient, free-stream dry and wet bulb temperatures, base temperature, and thermophysical properties are considered as constant. The mass deposition occurs everywhere on the frost surface, and the frost layer

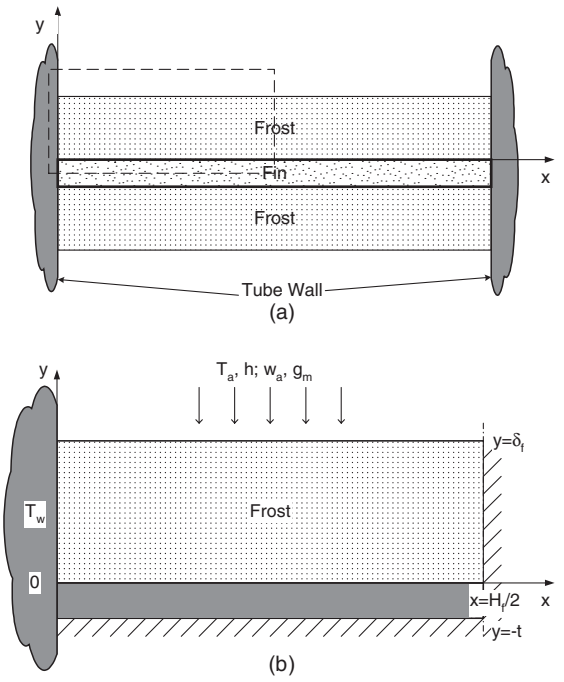

Fig. 7. A schematic of the frosted fin.

is assumed to be of uniform thickness. There is no contact resistance between the frost and the fin. The following assumptions are invoked: steady-state, two-dimensional conduction in frost layer on a one-dimensional fin, with no internal generation, and constant properties. With these assumptions, the fin temperature T_{fi} is a function of x only, and the frost temperature is $T_{\mathrm{f}}(x,y)$.

The governing equations for the temperature distribution are

$$k_{\mathrm{fi}}t\frac{\mathrm{d}^2T_{\mathrm{fi}}}{\mathrm{d}x^2}+k_{\mathrm{f}}\left.\frac{\partial T_{\mathrm{f}}}{\partial y}\right|_{y=0}=0 \quad \text{in } 0<x<H_{\mathrm{f}}/2 \tag{A.1a}$$

and

$$\frac{\partial^2T_{\mathrm{f}}}{\partial x^2}+\frac{\partial^2T_{\mathrm{f}}}{\partial y^2}=0 \quad \text{in } 0<x<H_{\mathrm{f}}/2,\ 0<y<\delta_{\mathrm{f}}, \tag{A.1b}$$

subject to

$$\left.\frac{\mathrm{d}T_{\mathrm{fi}}}{\mathrm{d}x}\right|_{x=H_{\mathrm{f}}/2}=0,\quad \left.\frac{\partial T_{\mathrm{f}}}{\partial x}\right|_{x=H_{\mathrm{f}}/2}=0, \tag{A.2a}$$

$$T_{\mathrm{fi}}(0)=T_{\mathrm{w}},\quad T_{\mathrm{f}}(0,y)=T_{\mathrm{w}}, \tag{A.2b}$$

$$T_{\mathrm{fi}}(x)=T_{\mathrm{f}}(x,0), \tag{A.2c}$$

and

$$\left.\frac{\partial T_{\mathrm{f}}}{\partial y}\right|_{y=\delta_{\mathrm{f}}}=\frac{h}{k_{\mathrm{f}}}(T_{\mathrm{a}}-T_{\mathrm{f}}(x,\delta_{\mathrm{f}}))+\frac{h_{\mathrm{sg}}g_{\mathrm{m}}}{k_{\mathrm{f}}}(\varpi_{\mathrm{a}}-\varpi_{\mathrm{fs}}(x,\delta_{\mathrm{f}})), \tag{A.2d}$$

where ω_{fs} is the saturated humidity ratio corresponding to $T_{\mathrm{f}}(x,\delta_{\mathrm{f}})$. Note that the fully frosted condition implies that ω_{a} is always bigger than ω_{fs}. If there is no mass transfer between the air and the frost, Eq. (A.2d) should be replaced by

$$\left.\frac{\partial T_{\mathrm{f}}}{\partial y}\right|_{y=\delta_{\mathrm{f}}}=\frac{h}{k_{\mathrm{f}}}(T_{\mathrm{a}}-T_{\mathrm{f}}(x,\delta_{\mathrm{f}})). \tag{A.3}$$

Xia and Jacobi [10] provided the analytical solution to Eqs. (A.1) subject to (A.2a)–(A.2c), and (A.3). The full series solution is

$$\frac{T_{\mathrm{f}}(x,y)-T_{\mathrm{a}}}{T_{\mathrm{w}}-T_{\mathrm{a}}}=\sum_{n=1}^{\infty}C_n\left[\cos\left(\frac{\lambda_n y}{\delta_{\mathrm{f}}}\right)-\frac{k_{\mathrm{fi}}t}{k_{\mathrm{f}}\delta_{\mathrm{f}}}\lambda_n\sin\left(\frac{\lambda_n y}{\delta_{\mathrm{f}}}\right)\right]\times\cosh\left(\frac{\lambda_n(H_{\mathrm{f}}/2-x)}{\delta_{\mathrm{f}}}\right), \tag{A.4a}$$

with C_n calculated using Eq. (7b), and λ_n is the root of

$$\tan(\lambda_n)=\frac{k_{\mathrm{fi}}k_{\mathrm{f}}t}{\delta_{\mathrm{f}}(k_{\mathrm{f}}^2+hk_{\mathrm{fi}}t)}\left[\left(\frac{h\delta_{\mathrm{f}}^2}{k_{\mathrm{fi}}t}\right)\frac{1}{\lambda_n}-\lambda_n\right]. \tag{A.4b}$$

Eqs. (A.4) provide a basis for deriving fin efficiencies.

Fin efficiency in the HA-LMED method. Based on Eqs. (1) and (2), Eqs. (A.1) and (A.2) can be reduced to

$$k_{\mathrm{fi}}t\frac{\mathrm{d}^2i_{\mathrm{fi}}}{\mathrm{d}x^2}+k_{\mathrm{f}}\left.\frac{\partial i_{\mathrm{f}}}{\partial y}\right|_{y=0}=0 \quad \text{in } 0<x<H_{\mathrm{f}}/2, \tag{A.5a}$$

and

$$\frac{\partial^2i_{\mathrm{f}}}{\partial x^2}+\frac{\partial^2i_{\mathrm{f}}}{\partial y^2}=0 \quad \text{in } 0<x<H_{\mathrm{f}}/2,\ 0<y<\delta_{\mathrm{f}}, \tag{A.5b}$$

subject to the following boundary conditions:

$$\left.\frac{\mathrm{d}i_{\mathrm{fi}}}{\mathrm{d}x}\right|_{x=H_{\mathrm{f}}/2}=0,\quad \left.\frac{\partial i_{\mathrm{f}}}{\partial x}\right|_{x=H_{\mathrm{f}}/2}=0, \tag{A.6a}$$

$$i_{\mathrm{fi}}(0)=i_{\mathrm{w}},\quad i_{\mathrm{f}}(0,y)=i_{\mathrm{w}}, \tag{A.6b}$$

$$i_{\mathrm{fi}}(x)=i_{\mathrm{f}}(x,0) \tag{A.6c}$$

and

$$\left.\frac{\partial i_{\mathrm{f}}}{\partial y}\right|_{y=\delta_{\mathrm{f}}}=\frac{hb/c_{p_{\mathrm{a}}}}{k_{\mathrm{f}}}(i_{\mathrm{a}}-i_{\mathrm{f}}(x,\delta_{\mathrm{f}})), \tag{A.6d}$$

where $i_{\mathrm{fi}}(x)$ and $i_{\mathrm{f}}(x,y)$ are the saturated enthalpies of moist air at corresponding temperatures. Comparing Eqs. (A.5) and (A.6) to (A.1), (A.2a)–(A.2c) and (A.3), the solution is obtained by replacing the T's and h in Eqs. (A.4) with i's and $hb/c_{p_{\mathrm{a}}}$.

The total heat transfer per unit fin width to the fin surface is then calculated by

$$\frac{q_{\mathrm{fi,b}}}{L_{\mathrm{f}}}=4\left(k_{\mathrm{fi}}t/b\left.\frac{\mathrm{d}i_{\mathrm{fi}}}{\mathrm{d}x}\right|_{x=0}+\int_0^{\delta_{\mathrm{f}}}k_{\mathrm{f}}/b\left.\frac{\partial i_{\mathrm{f}}}{\partial x}\right|_{x=0}\mathrm{d}y\right). \tag{A.7}$$

Then, the fin efficiency defined by Eq. (6) is calculated to obtain Eq. (7).

Starting from the definition, Eq. (5), and considering the total heat transfer as comprised of $q_{\mathrm{fi,b}}$ and $q_{\mathrm{w,unf}}$, which are the heat transfer to the frosted fin surface and to the unfinned surface respectively, the surface efficiency is obtained as

$$\eta_{\mathrm{h}} = \frac{q_{\mathrm{fi,b}}}{A_{\mathrm{h}}(h_{\mathrm{h}}/c_{p_{\mathrm{a}}})(i_{\mathrm{a}} - i_{\mathrm{w,o}})} + \frac{q_{\mathrm{w,unf}}}{A_{\mathrm{h}}(h_{\mathrm{h}}/c_{p_{\mathrm{a}}})(i_{\mathrm{a}} - i_{\mathrm{w,o}})}. \quad \text{(A.8)}$$

For $q_{\mathrm{w,unf}}$, we have

$$q_{\mathrm{w,unf}} = (A_{\mathrm{h}} - A_{\mathrm{fi}})(h_{\mathrm{h}}/c_{p_{\mathrm{a}}})(i_{\mathrm{a}} - i_{\mathrm{fs,w}}). \quad \text{(A.9)}$$

Assuming one-dimensional heat conduction in the frost layer on the tube wall (normal to the tube wall), the saturated enthalpy corresponding to the temperature of the frost surface on the tube wall can be expressed as

$$i_{\mathrm{fs,w}} = \frac{i_{\mathrm{a}}(h_{\mathrm{h}}b/c_{p_{\mathrm{a}}}) + i_{\mathrm{w,o}}k_{\mathrm{f}}/\delta_{\mathrm{f}}}{(h_{\mathrm{h}}b/c_{p_{\mathrm{a}}}) + k_{\mathrm{f}}/\delta_{\mathrm{f}}}. \quad \text{(A.10)}$$

Substituting Eqs. (6), (A.9), and (A.10) into Eq. (A.8), the expression for overall surface efficiency, Eq. (10), is obtained.

Fin efficiency in the UA-LMTD method. Here the mass transfer effects are included in the convective heat transfer coefficient h by utilizing the assumption of constant sensible heat ratio. Eqs. (A.1) and (A.2) remain unchanged, except that the last boundary condition, Eq. (A.2d) becomes

$$\left.\frac{\partial T_{\mathrm{f}}}{\partial y}\right|_{y=\delta_{\mathrm{f}}} = \frac{hq_{\mathrm{a}}/q_{\mathrm{a,s}}}{k_{\mathrm{f}}}(T_{\mathrm{a}} - T_{\mathrm{f}}(x,\delta_{\mathrm{f}})). \quad \text{(A.11)}$$

The solution can be easily obtained by replacing the h in Eqs. (A.4) with $hq_{\mathrm{a}}/q_{\mathrm{a,s}}$. The details of the derivation are omitted.

If mass transfer effects are to be isolated, and a linear relation between the saturated humidity ratio and temperature from fin tip to base is assumed, then the last boundary condition, Eq. (A.2d), is rewritten as

$$\left.\frac{\partial T_{\mathrm{f}}}{\partial y}\right|_{y=\delta_{\mathrm{f}}} = \frac{h}{k_{\mathrm{f}}}(T_{\mathrm{a}} - T_{\mathrm{f}}(x,\delta_{\mathrm{f}})) + \frac{h_{\mathrm{sg}}g_{\mathrm{m}}}{k_{\mathrm{f}}}[(\varpi_{\mathrm{a}} - \varpi_{\mathrm{a,sat}}) + (\varpi_{\mathrm{a,sat}} - \varpi_{\mathrm{fs}}(x,\delta_{\mathrm{f}}))], \quad \text{(A.12)}$$

where $\omega_{\mathrm{a,sat}}$ is the saturated humidity ratio corresponding to the temperature of the moist air. Noting that $(\omega_{\mathrm{a}} - \omega_{\mathrm{a,sat}})$ is constant, and using Eqs. (33) and (A.12) becomes

$$\left.\frac{\partial T_{\mathrm{f}}}{\partial y}\right|_{y=\delta_{\mathrm{f}}} = \frac{h'}{k_{\mathrm{f}}}(T'_{\mathrm{a}} - T_{\mathrm{f}}(x,\delta_{\mathrm{f}})), \quad \text{(A.13)}$$

with

$$h' = h\left(1 + \frac{h_{\mathrm{sg}}g_{\mathrm{m}}e}{h}\right) \quad \text{(A.14)}$$

and

$$T'_{\mathrm{a}} = T_{\mathrm{a}} + \frac{h_{\mathrm{sg}}g_{\mathrm{m}}/h}{1 + h_{\mathrm{sg}}g_{\mathrm{m}}e/h}(\varpi_{\mathrm{a}} - \varpi_{\mathrm{a,sat}}). \quad \text{(A.15)}$$

The solution to Eqs. (A.1) and (A.2) with (A.13) substituted for (A.2d) can be easily obtained by replacing h and T_{a} in Eqs. (A.4) with h' and T'_{a}.

The total heat transfer to the fin surface per unit fin width is then calculated by

$$\frac{q_{\mathrm{fi,b}}}{L_{\mathrm{f}}} = 4\left(k_{\mathrm{fi}}t\left.\frac{\mathrm{d}T_{\mathrm{fi}}}{\mathrm{d}x}\right|_{x=0} + \int_0^{\delta_{\mathrm{f}}} k_{\mathrm{f}}\left.\frac{\partial T_{\mathrm{f}}}{\partial x}\right|_{x=0}\mathrm{d}y\right). \quad \text{(A.16)}$$

The maximum heat transfer is (were the fin surface at the base temperature)

$$\frac{q_{\max}}{L_{\mathrm{f}}} = 2H_{\mathrm{f}}\left[h(T_{\mathrm{a}} - T_{\mathrm{w}}) + h_{\mathrm{sg}}g_{\mathrm{m}}(\varpi_{\mathrm{a}} - \varpi_{\mathrm{w,sat}})\right] = 2H_{\mathrm{f}}h'(T'_{\mathrm{a}} - T_{\mathrm{w}}). \quad \text{(A.17)}$$

Thus, the fin efficiency is calculated yielding Eq. (34).

References

[1] C. Sanders, The influence of frost formation and defrosting on the performance of air coolers, Ph.D. Dissertation, Technische Hogescool, Delft, Netherlands, 1974.

[2] S.N. Kondepudi, D.L. O'Neal, Effect of frost growth on the performance of louvered finned tube heat exchangers, Int. J. Refrig. 12 (1989) 151–158.

[3] P.J. Mago, S.A. Sherif, Modeling the cooling process path of a dehumidifying coil under frosting conditions, J. Heat Transfer 124 (2002) 1182–1191.

[4] K. Ogawa, N. Tanaka, M. Takeshita, Performance improvement of plate fin-and-tube heat exchangers under frosting conditions, ASHRAE Trans. 99 (1993) 762–774.

[5] W.F. Stoecker, Frost formation on refrigeration coils, ASHRAE Trans. 66 (1960) 91–103.

[6] H. Barrow, A note on frosting of heat pump evaporator surfaces, J. Heat Recovery Syst. 5 (1985) 195–201.

[7] G.D. Huffman, C.F. Sepsy, Heat transfer and pressure loss in extended surface heat exchangers operating under frosting conditions—Part II: Data analysis and correlation, ASHRAE Trans. 73 (1967) 1.3.1–1.3.16.

[8] D.H. Niederer, Frosting and defrosting effects on coil heat transfer, ASHRAE Trans. 82 (1976) 467–473.

[9] G. Wu, T.-Y. Bong, Overall efficiency of a straight fin with combined heat and mass transfer, ASHRAE Trans. 100 (1994) 367–374.

[10] Y. Xia, A.M. Jacobi, An exact solution to steady heat conduction in a two-dimensional slab on a one-dimensional fin: application to frosted heat exchangers, Int. J. Heat Mass Transfer 47 (2004) 3317–3326.

[11] S.N. Kondepudi, D.L. O'Neal, A simplified model of pin fin heat exchangers under frosting conditions, ASHRAE Trans. 99 (1993) 754–761.

[12] W.F. Stoecker, J.W. Jones, Refrigeration and Air Conditioning, 2nd ed., McGraw-Hill, Inc., 1982, pp. 54–55.

[13] S.N. Kondepudi, D.L. O'Neal, The effects of frost growth on extended surface heat exchanger performance: a review, ASHRAE Trans. 93 (1987) 258–274.